# Kinetic Evaluation of Catalase and Peroxygenase Activities of Tyrosinase†

Shin-ichi Yamazaki, Chiyuki Morioka, and Shinobu Itoh*

*Department of Chemistry, Graduate School of Science, Osaka City University, 3-3-138 Sugimoto, Sumiyoshi-ku, Osaka 558-8585, Japan*

*Received May 28, 2004; Revised Manuscript Received July 6, 2004*

ABSTRACT: Tyrosinase is a copper monooxygenase containing a coupled dinuclear copper active site (type-3 copper), which catalyzes oxygenation of phenols (phenolase activity) as well as dehydrogenation of catechols (catecholase activity) using $O_2$ as the oxidant. In this study, catalase activity (conversion of $H_2O_2$ to $(1/2)O_2$ and $H_2O$) and peroxygenase activity ($H_2O_2$-dependent oxygenation of substrates) of mushroom tyrosinase have been examined kinetically by using amperometric $O_2$ and $H_2O_2$ sensors. The catalase activity has been examined by monitoring the initial rate of $O_2$ production from $H_2O_2$ in the presence of a catalytic amount of tyrosinase in 0.1 M phosphate buffer (pH 7.0) at 25 °C under initially anaerobic conditions. It has been found that the catalase activity of mushroom tyrosinase is three-order of magnitude greater than that of mollusk hemocyanin. The higher catalase activity of tyrosinase could be attributed to easier accessibility of $H_2O_2$ to the dinuclear copper site of tyrosinase. Mushroom tyrosinase has also been demonstrated for the first time to catalyze oxygenation reaction of phenols with $H_2O_2$ (peroxygenase activity). The reaction has been investigated kinetically by monitoring the $H_2O_2$ consumption rate in 0.5 M borate buffer (pH 7.0) under aerobic conditions. Similarity of the substituent effects of a series of *p*-substituted phenols in the peroxygenase reaction with $H_2O_2$ to those in the phenolase reaction with $O_2$ as well as the absence of kinetic deuterium isotope effect with a perdeuterated substrate (*p*-Cl-$C_6D_4OH$ vs *p*-Cl-$C_6H_4OH$) clearly demonstrated that the oxygenation mechanisms of phenols in both systems are the same, that is, the electrophilic aromatic substitution reaction by a ($\mu$-$\eta^2$:$\eta^2$-peroxo)-dicopper(II) intermediate of oxy-tyrosinase.

Tyrosinase (EC 1.14.18.1) is a copper monooxygenase widely distributed throughout bacteria, fungi, plants, and animals. The enzyme catalyzes oxygenation of phenols to catechols by $O_2$ (so-called phenolase activity) as well as dehydrogenation of catechols to the corresponding *o*-quinones (catecholase activity) (*1*, *2*). The *o*-quinone products thus produced are spontaneously converted into melanin pigments via nonenzymatic reaction pathways (*3*). Tyrosinase has a coupled dinuclear copper active site (classified as type-3) like catechol oxidase (EC 1.10.3.1), ubiquitous plant enzyme catalyzing the oxidation of a broad range of catechols to the corresponding *o*-quinones, and hemocyanin acting as an oxygen carrier and storage protein in mollusks and arthropods (*4*). The oxy-forms of these enzymes (proteins) involve similar side-on ($\mu$-$\eta^2$:$\eta^2$) peroxo dicopper(II) species, but exhibit different chemical reactivity and functions.

In tyrosinase, the peroxo intermediate has been suggested to perform the previous oxidation reactions (phenol oxygenation and catechol dehydrogenation), generating an hydroxo-bridged dicopper(II) species (met-form) as the resting state of enzyme (*1*). Met-tyrosinase also reacts with catechols to give the corresponding *o*-quinone products and deoxy-tyrosinase (dicopper(I) form), from which oxy-tyrosinase is regenerated by the reaction with $O_2$ completing the catalytic cycle (*1*−*7*). Catechol oxidase, on the other hand, exhibits only the catecholase activity (catechol dehydrogenation), presumably due to the limited space for substrate binding. Namely, the substrate-binding site of catechol oxidase may not be suited for binding of phenols in the proper orientation required for the oxygen atom transfer process (phenolase activity) (*8*−*10*). In contrast to the case of tyrosinase and catechol oxidase, hemocyanin possesses only a reversible dioxygen binding ability. The lack of redox reactivity of hemocyanin toward external substrates has been attributed to the absence of substrate-binding site around the dinuclear copper site (*11*).

Thus, tyrosinase exhibits a unique function, oxygen atom transfer from the peroxo intermediate of oxy-tyrosinase to the phenol substrates, which is the most attractive process among the catalytic mechanism of tyrosinase from the viewpoint of dioxygen activation chemistry. Although the crystal structure of tyrosinase has yet to be obtained, geometric discussion based on the X-ray structures of catechol oxidase and hemocyanin has provided profound insights into the catalytic mechanism of tyrosinase (*8*−*11*). Spectroscopic studies of tyrosinase have also provided important information on the catalytic intermediates of the enzymatic reactions (*1*, *12*−*14*). However, detailed mechanistic study on the oxygen atom transfer process (phenolase activity) had not been accomplished until recently due to the large influences of concomitantly occurring catechol dehydrogenation (catecholase activity) and the melanin

† Supported by Grants-in-Aid for Scientific Research from the Ministry of Education, Science, Sports, and Culture of Japan (15350105) and Research Fellowships of Japan Society for the Promotion of Science for Young Scientists.

* To whom correspondence should be addressed. Phone and fax: +81-6-6605-2564; e-mail: shinobu@sci.osaka-cu.ac.jp.

10.1021/bi048908f CCC: $27.50 
Published on Web 08/20/2004

Scheme 1: Electrophilic Aromatic Substitution Mechanism for the Oxygen Atom Transfer Process from a ($\mu$-$\eta^2$:$\eta^2$-Peroxo)dicopper(II) Species to a Phenol Substrate (*19*)

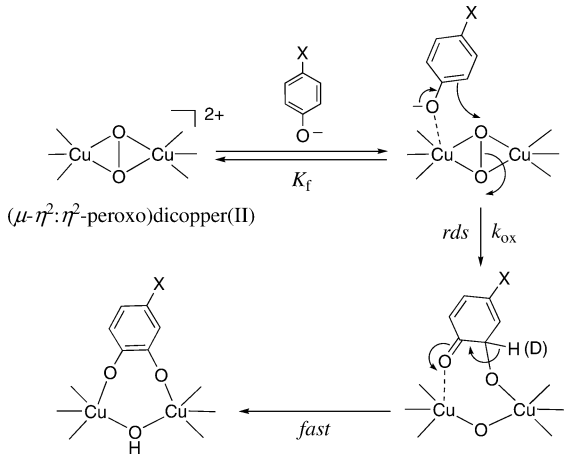


production (*2*, *3*, *15*−*17*). In this regard, we have recently succeeded to develop a very simple enzymatic reaction system using a borate buffer as a trapping agent of catechols and hydroxylamine as an external reductant. The simplified catalytic reaction system allowed us to examine the phenolase activity of tyrosinase without interference of the catecholase activity and the melanin formation reactions (*18*). Direct comparison of the electronic effects of *p*-substituents of a series of phenol substrates in the simplified enzymatic reaction to those in our tyrosinase model reaction (*19*) has clearly demonstrated that electrophilic aromatic substitution reaction is the most plausible mechanism for the oxygenation of phenols by the ($\mu$-$\eta^2$:$\eta^2$-peroxo)dicopper(II) intermediate (Scheme 1) as previously suggested by others using a related model reaction (an aromatic ligand hydroxylation in a dicopper(I) complex with $O_2$) (*20*, *21*).

In the native enzymatic reaction, the ($\mu$-$\eta^2$:$\eta^2$-peroxo)-dicopper(II) active species (oxy form) is generated by the reaction of $O_2$ and deoxy-tyrosinase (dicopper (I) form), which is generated by the reduction of met-tyrosinase (dicopper (II) form) with catechol products. In the absence of substrates, the ($\mu$-$\eta^2$:$\eta^2$-peroxo)dicopper(II) species can be also generated by the reaction of met-tyrosinase and $H_2O_2$, the so-called shunt path (*22*−*24*). For the spectroscopic characterization of the peroxo intermediate of oxy-tyrosinase, the later method, oxidation of met-tyrosinase by $H_2O_2$, has been generally employed (*22*−*25*). However, little attention has so far been paid on the mechanistic aspect of the $H_2O_2$ oxidation of met-tyrosinase.

On the other hand, catalase activity (conversion of $H_2O_2$ to (1/2)$O_2$ and $H_2O$) of hemocyanin has been investigated to add some insights into the biological functions of hemocyanin (*26*−*29*). Krebs and co-workers recently reported a catalase-like activity of the isozymes of catechol oxidase and proposed a $H_2O_2$ degradation mechanism based on the X-ray structure of catechol oxidase (*30*). The catalase activity of tyrosinase was also reported by Mason and co-workers a long time ago (*23*), but quantitative measurements and detailed mechanistic studies on the catalase activity of tyrosinase has yet to be performed. With regard to the peroxidase activity of tyrosinase ($H_2O_2$-dependent oxidation of substrates), Mason and co-workers also reported the oxidation of *p*-phenylendiamine by $H_2O_2$ very briefly (*23*). However, detailed study of the peroxidase activity has not been carried out either. The lack of mechanistic studies of the catalase and peroxidase activity of tyrosinase may be due to difficulties in quantitative monitoring of $H_2O_2$ consumption and/or $O_2$ generation during the enzymatic reactions. The peroxidase activity could be evaluated by monitoring the time course of the substrate consumption and/or product formation. However, this is also quite difficult due to the interference by the inherent phenolase activity and catecholase activity.

We report herein quantitative evaluation of catalase and peroxygenase activity[1] of mushroom tyrosinase using amperometric methods to overcome the previously mentioned problems. Detailed steady-state kinetic analysis on the catalase activity has been performed by monitoring the $O_2$ formation rate using a Clark-type oxygen electrode connected to a closed cell. Furthermore, the phenol oxygenation by $H_2O_2$ (peroxygenase activity) has been quantitatively analyzed for the first time by using a bioelectrochemical $H_2O_2$ sensor, with which we can determine the $H_2O_2$ consumption rate accurately even in the presence of a large excess of phenols (substrate) and catechols (product) (*31*, *32*). The peroxygenase activity was examined in a borate buffer, in which the catechol products are trapped by the complex formation with borate ion (*32*, *33*), preventing the interference by the catecholase activity (over oxidation of phenols) as in the case of our previous study on the phenolase activity (oxygenation of phenols with $O_2$) (*18*). Quantitative analysis on the substituent effects of a series of *p*-substituted phenols in the peroxygenase activity has demonstrated that the reaction mechanism is the same to that of the phenolase reaction, that is, the electrophilic aromatic substitution mechanism (Scheme 1) (*18*, *19*).

## EXPERIMENTAL PROCEDURES

*Materials.* All chemical reagents used in this study, except *p*-Cl-$C_6D_4OH$, were commercial products of the highest available purity and were used as received. Mollusk (*Concholepas concholepas*) hemocyanin was purchased from Sigma and was used as received. The deuterated phenol, *p*-Cl-$C_6D_4OH$, was prepared according to the reported procedure (*34*), and its purity (more than 99%) was confirmed by $^1$H NMR and MS analyses using a JEOL FT-NMR Lambda 300WB and a JEOL JMS-700T Tandem MS-station mass spectrometer, respectively.

*Purification of Tyrosinase from Cell-Free Extract of Mushroom.* A cell-free extract of mushroom (*Agaricus bisporous*) was prepared by the procedure described in the Supporting Information of our previous paper (*18*), except for a little modification, in which an ice-cold borate buffer solution (0.5 M, pH 9.0) was used for the extraction of proteins in place of ice-cold water to prevent polymerization of endogenous phenols. Purification of tyrosinase and preparation of oxy-tyrosinase were also performed by the same methods described in the Supporting Information of our previous paper (*18*). The concentration of tyrosinase was determined by using the adsorption change at 345 nm [$\epsilon$ = 18000 $M^{-1}$ $cm^{-1}$, for ($\mu$-$\eta^2$:$\eta^2$-peroxo)dicopper(II) form] (*23*) of the difference spectrum

[1] The term peroxygenase activity is used instead of peroxidase activity since the present reaction involves a peroxide ($H_2O_2$)-dependent oxygenation reaction (cf. Ozaki, S., Roach, M. P., Matsui, T., and Watanabe, Y. (2001) Investigations of the roles of the distal heme environment and the proximal heme iron ligand in peroxide activation by heme enzymes via molecular engineering of myoglobin, *Acc. Chem. Res. 34*, 818−825).

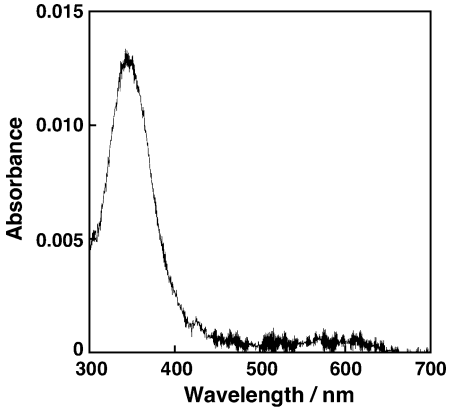


FIGURE 1: Difference spectrum obtained by subtracting a spectrum of met-tyrosinase from that of oxy-tyrosinase generated by the addition of 9.2 $\mu$M $H_2O_2$ to met-tyrosinase in 0.1 M phosphate (pH 7.0) under air-saturated conditions at 25 °C.

obtained under the $O_2$-saturated conditions. Concentration of the purified tyrosinase was also determined by Lowry method. The concentrations estimated by the two independent ways were roughly the same.

*Deactivation of Tyrosinase.* Deactivation of tyrosinase was performed by incubating a tyrosinase solution at 80 °C for 5 min before use.

*Monitoring of $O_2$ Concentration.* Time courses of $O_2$ concentration change were monitored by an ALS 630A electrochemical analyzer using a Clark-type oxygen electrode connected to a closed cell (Central Kagaku Co. Ltd.). Applied potential was −0.6 V versus Ag/AgCl/KCl (1.0 M). The electrochemical measurements were performed at 25 °C in 0.1 M phosphate buffer (pH 7.0).

*Monitoring of $H_2O_2$ Concentration.* The amperometric monitoring of $H_2O_2$ was performed using an ALS 630A electrochemical analyzer equipped with a bioelectrochemical $H_2O_2$ sensor, which consists of horseradish peroxidase entrapped on a carbon paste electrode surface with cellulose ester dialysis membrane. The carbon paste electrode was made by embedding ferrocene into the carbon paste. The detailed fabrication procedure of the $H_2O_2$ sensor was described in the literature (*31*). Applied potential was 0.1 V versus Ag/AgCl/KCl (1.0 M). The electrochemical measurements were performed at 25 °C in 0.5 M borate buffer (pH 7.0) under $O_2$-saturated conditions.

*Product Analysis.* Catechol products of the phenol oxygenation reaction with $H_2O_2$ were analyzed by an HPLC system consisting of a Shimadzu LC-6A chromatographic pump, a Shimadzu UV−vis spectrophotometric detector SPD-6AV, and an ODS column (Prodigi 250 × 4.6 mm, Phenomenex) with a mobile phase of acetonitrile/water = 65:35, containing 0.1% trifluoroacetic acid at a constant flow rate of 0.3 mL $min^{-1}$.

## RESULTS AND DISCUSSION

*Catalase Activity of Mushroom Tyrosinase.* Most of tyrosinase purified from mushroom exists as the met-form (*22*), from which oxy-tyrosinase, the ($\mu$-$\eta^2$:$\eta^2$-peroxo)-dicopper(II) form, can be generated by the treatment with $H_2O_2$ under aerobic conditions (*22*−*24*). A typical example of the UV−vis spectrum of oxy-tyrosinase thus generated is shown in Figure 1. The spectrum of oxy-tyrosinase, however, slowly decayed even in the presence of an excess amount of $H_2O_2$ as previously reported by Mason et al (*23*). This may be due to consumption of $H_2O_2$ in the solution by the catalase activity of tyrosinase as proposed by the authors (*23*). However, there has been no report of detailed analysis on the catalase activity of tyrosinase. Thus, we first tried to evaluate the catalase activity of mushroom tyrosinase by monitoring the $O_2$-production rate using a Clark-type oxygen electrode.

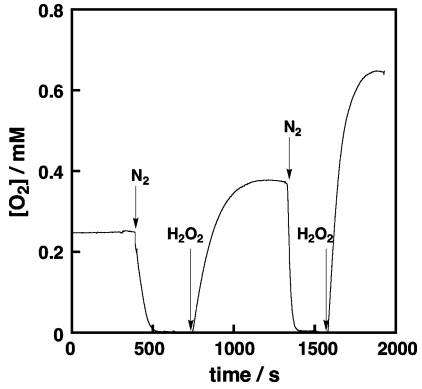


FIGURE 2: Time course of $O_2$ generation due to the catalase activity of tyrosinase. The measurement was performed in 0.1 M phosphate buffer (pH 7.0) containing tyrosinase (0.6 $\mu$M) at 25 °C. The concentrations of added $H_2O_2$ were 0.61 and 1.51 mM, respectively.

To simplify the catalytic reaction of catalase activity, we performed the kinetic analysis under initially anaerobic conditions by using a closed cell equipped with the oxygen electrode. Thus, a 0.1 M phosphate buffer solution (pH 7.0) containing met-tyrosinase (0.6 $\mu$M) was deaerated by flushing $N_2$ gas until the $O_2$ concentration became virtually zero as shown in Figure 2. Then, an aliquot of a deaerated $H_2O_2$ stock solution of the same buffer was added into the tyrosinase solution ($[H_2O_2]_{add}$ = 0.61 mM), where $O_2$ concentration increased with time and reached a constant value of 0.38 mM. The concentration of generated $O_2$ was approximately half of the added $H_2O_2$ concentration, indicating that almost all $H_2O_2$ added into the solution was decomposed into $O_2$ (0.5 equiv) and $H_2O$ as indicated in eq 1. Since no $O_2$ generation was detected with a heat-treated tyrosinase (denatured enzyme), the $O_2$ production shown in Figure 2 was attributed to the catalase activity of tyrosinase itself but not to $H_2O_2$ degradation by impurities such as metal ions released from the enzyme active site.

$$H_2O_2 \rightarrow (1/2)O_2 + H_2O \quad (1)$$

After the $O_2$ generation was completed, $N_2$ gas was flushed again to make the solution deaerated, to which another aliquot of the $H_2O_2$ solution ($[H_2O_2]_{add}$ = 1.51 mM) was added to cause the $O_2$ generation again (Figure 2). The apparent rate of catalase activity ($v^c$) was then determined from the initial slope of each $O_2$-generation curve at a different initial $H_2O_2$ concentration. In Figure 3 is shown the plot of $v^c$ versus initial $H_2O_2$ concentration, where a linear correlation was observed in the wide rage of $[H_2O_2]$ examined.

A plausible mechanism of the catalase activity is shown in Scheme 2. Reaction of met-tyrosinase with $H_2O_2$ generates oxy-tyrosinase, ($\mu$-$\eta^2$:$\eta^2$-peroxo)dicopper(II) species, from which $O_2$ is released to give deoxy-tyrosinase (dicopper(I) form) under the low $[O_2]$ conditions. The generated deoxy-tyrosinase is then oxidized by another molecule of $H_2O_2$ to produce $H_2O$ and met-tyrosinase completing the catalytic cycle. The first two processes, formation of oxy-tyrosinase from met-tyrosinase by the reaction with $H_2O_2$ and $O_2$ release from oxy-tyrosinase to give deoxy-tyrosinase, are well-documented in the literature (*23*). Although the third process,

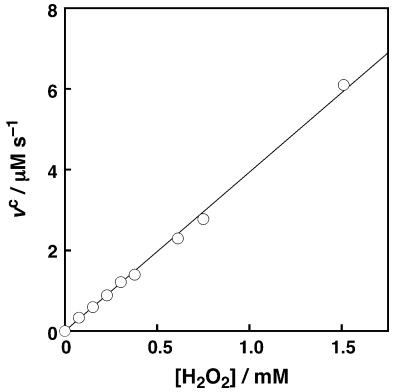


FIGURE 3: Plot of $v^c$ ($O_2$-production rate) against $H_2O_2$ concentration for the catalase activity of mushroom tyrosinase (0.6 $\mu$M). The reaction conditions are those described in Figure 2.

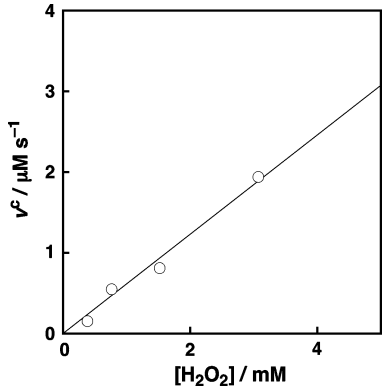


FIGURE 4: Plot of $v^c$ ($O_2$-production rate) against $H_2O_2$ concentration for the catalase activity of mollusk hemocyanin (77 $\mu$M). The reaction conditions are similar to those described in Figure 2.

Scheme 2: Proposed Catalytic Mechanism of Catalase Activity of Tyrosinase

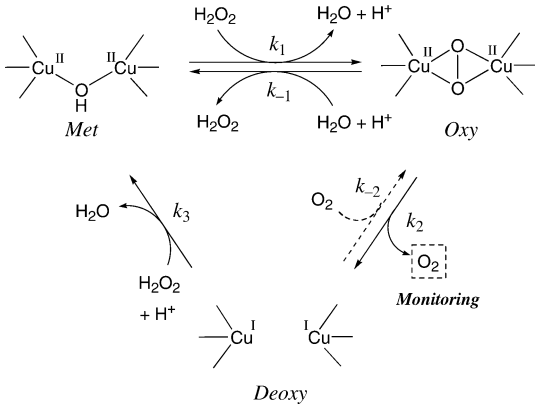


oxidation of deoxy-tyrosinase to met-tyrosinase by $H_2O_2$, has yet to be reported, a similar reaction (conversion of deoxy-form to met-form by $H_2O_2$) has recently been demonstrated with hemocyanin (*29*). In our model study, reaction of a copper(I) complex with $H_2O_2$ also gave a ($\mu$-$\eta^2$:$\eta^2$-peroxo)-dicopper(II) complex, also supporting accuracy of the mechanism shown in Scheme 2 (*35*). Therefore, the spectrum shown in Figure 1 can be ascribed to the peroxo species that existed as a steady-state intermediate of the catalytic reaction of catalase activity, and the peroxo intermediate gradually disappears when $H_2O_2$ is consumed by the catalase reaction. The kinetic equation derived based on Scheme 2 is shown in eq 2, where the $O_2$-binding process to deoxy-tyrosinase ($k_{-2}$ process) was neglected since the reaction was carried out under initially anaerobic conditions ([$O_2$] $\sim$ 0; the $k_{-2}$ process becomes important when the reaction is carried out under aerobic conditions as described next).

$$v^c = \frac{V_{max}[H_2O_2]}{[H_2O_2] + K_M} \qquad (2)$$

$$V_{max} = k_2[E]$$

$$K_M = \frac{k_2(k_1 + k_3)}{k_1 k_3} + \frac{k_{-1}}{k_1}$$

The linear correlation between $v^c$ versus [$H_2O_2$] shown in Figure 3 strongly indicates that the $K_M$ value is sufficiently larger than [$H_2O_2$], simplifying eq 2 as $v^c = (V_{max}[H_2O_2])/K_M$. In addition, if the $O_2$-dissociation process from oxy-tyrosinase ($k_2$) is sufficiently faster than the other processes ($k_1$ and $k_{-1}$ for the reversible $H_2O_2$-binding process and $k_3$ for the oxidation process of deoxy-tyrosinase by $H_2O_2$), eq 2 can be further simplified as eq 3

$$v^c = \frac{V_{max}[H_2O_2]}{K_M} = \frac{k_1 k_3}{k_1 + k_3}[H_2O_2][E] \qquad (3)$$

Thus, the apparent bimolecular rate constant between $H_2O_2$ and tyrosinase was determined as $6.6 \times 10^3$ $M^{-1}$ $s^{-1}$ by dividing the slope of linear line in Figure 3 by the concentration of tyrosinase [E].

*Comparison of Catalase Activity between Tyrosinase and Hemocyanin.* Catalase activity of mollusk hemocyanin has been already examined, even though the reaction was carried out at higher $H_2O_2$ concentrations (*26*, *27*). In this study, we have reexamined the catalase activity of mollusk hemocyanin by using our present method to compare the catalase activity between tyrosinase and hemocyanin under the same experimental conditions. As shown in Figure 4, linear dependence of the catalase activity of hemocyanin ($v^c$) on the $H_2O_2$ concentration was also observed, from which the apparent bimolecular rate constant was calculated as 8.0 $M^{-1}$ $s^{-1}$ in the same way. The results clearly indicate that the catalase activity of tyrosinase ($6.6 \times 10^3$ $M^{-1}$ $s^{-1}$) is three orders of magnitude higher than that of mollusk hemocyanin (8.0 $M^{-1}$ $s^{-1}$). It was suggested that the reaction between met-hemocyanin and $H_2O_2$ is very slow, being the rate-limiting step of the catalase activity (*27*). In this context, the reaction between $H_2O_2$ and met-tyrosinase may be much faster than the hemocyanin case, resulting in the higher catalase activity of tyrosinase.

The spectral information supported this notion as follows. In the case of hemocyanin, the addition of an excess amount of $H_2O_2$ into met-hemocyanin decreases the absorption band of oxy-hemocyanin (*27*), which is due to acceleration of the $k_3$ process (oxidation of deoxy-hemocyanin to met-hemocyanin by $H_2O_2$). Namely, the oxy-hemocyanin, generated by the slow reaction between met-hemocyanin and $H_2O_2$, is consumed readily in the presence of a large excess of $H_2O_2$ due to acceleration of the $k_3$ process. In the case of tyrosinase, on the other hand, even in the presence of an excess amount of $H_2O_2$, the spectrum of oxy-tyrosinase is still observed (Figure 1). This could be attributed to the fast regeneration

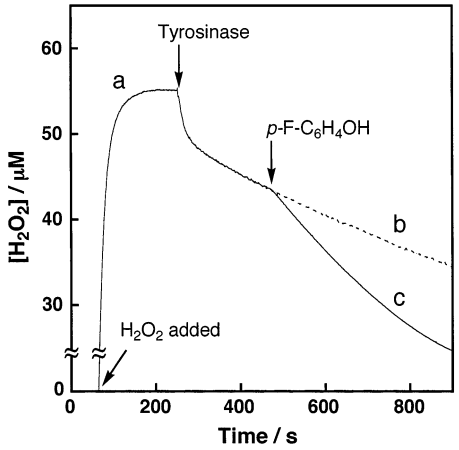


FIGURE 5: Time course of $H_2O_2$ concentration change observed in the peroxygenase reaction of mushroom tyrosinase. [Tyrosinase] = 0.135 $\mu$M, [*p*-F-$C_6H_4OH$] = 91.4 $\mu$M in 0.5 M borate buffer (pH 7.0) under $O_2$-saturated conditions at 25 °C.

of oxy-tyrosinase from met-tyrosinase by the efficient reaction with $H_2O_2$. Although the crystal structure of tyrosinase has yet to be obtained, comparison of the crystal structures between hemocyanin (*36*, *37*) and catechol oxidase (*8.9*) has indicated that catechol oxidase has a larger space around the dicopper active site for the substrate binding, while the active site of hemocyanin is blocked by the amino acid side chain such as Leu 2830 to prevent the access of the external substrate. Thus, the difference in catalase activity between tyrosinase and hemocyanin could be attributed to the difference of accessibility of $H_2O_2$ into the dicopper active site of met-protein.

*Peroxygenase Activity of Mushroom Tyrosinase.* Mason and co-workers reported a peroxidase activity of mushroom tyrosinase (oxidation of *p*-phenylendiamine with $H_2O_2$) very briefly (*23*). In the present study, we have also investigated tyrosinase-catalyzed oxygenation of a series of *p*-substituted phenols by $H_2O_2$. In this case, the products will be catechols, so that the reaction can be referred to peroxygenase activity.[1] In principle, tyrosinase will be able to catalyze the oxygenation of phenols by $H_2O_2$ since the reaction of met-tyrosinase and $H_2O_2$ produces the ($\mu$-$\eta^2$:$\eta^2$-peroxo)dicopper(II) intermediate, the active species for the native phenolase activity of tyrosinase (vide ante).

When *p*-chlorophenol (282 $\mu$M) was treated with $H_2O_2$ (263 $\mu$M) in 1.0 M borate buffer (pH 7.0) in the presence of a catalytic amount of mushroom tyrosinase (0.55 $\mu$M) for 30 min under aerobic conditions, 4-chlorocatechol was produced in 86% based on the initial $H_2O_2$ concentration (detected by HPLC). The result unambiguously demonstrated that tyrosinase exhibits peroxygenase activity as we expected. Then, the reaction was investigated kinetically using the $H_2O_2$-sensor (see Experimental Procedures) under the experimental conditions described in Figure 5. Contrary to the case of catalase activity, the peroxygenase activity was examined under $O_2$-saturated conditions to diminish the $O_2$-dissociation process from oxy-tyrosinase to deoxy-tyrosinase; $k_{-2}[O_2] > k_2$ (see Scheme 2). Furthermore, the borate buffer was employed instead of the phosphate buffer to prevent the catecholase activity as in the case of our previous study of phenolase activity (*18*). Under these experimental conditions, the phenolase activity of tyrosinase was negligible since no

Scheme 3: Proposed Catalytic Mechanism of Peroxygenase Activity of Tyrosinase

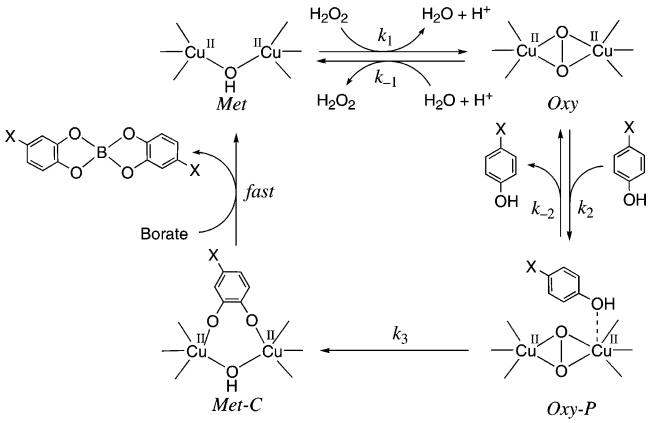


$O_2$ consumption was detected during the catalytic reaction (confirmed by following with the $O_2$ sensor).

In Figure 5 is shown the time course of $H_2O_2$ concentration change in the reaction. When $H_2O_2$ was added into an $O_2$-saturated borate buffer solution, the cathodic current immediately increased to reach a constant value (line a). Addition of a borate buffer of tyrosinase into the $H_2O_2$ solution caused a rapid decrease of the cathodic current that was followed by the slow decrease of $H_2O_2$ concentration (line b). The initial rapid decrease of the cathodic current is due to dilution of the $H_2O_2$ solution by the addition of tyrosinase stock solution, and the following slow decrease is attributed to the catalase activity of tyrosinase described previously. Thus, the catalase activity of tyrosinase has been confirmed not only by the increase of $O_2$ concentration (Figure 2) but also the decrease of $H_2O_2$ concentration (Figure 5, line b). Then, the phenol substrate was added into the $H_2O_2$ solution containing tyrosinase to cause an acceleration of $H_2O_2$ consumption rate (line c) due to the peroxygenase activity. The rate of peroxygenase reaction ($v^p$) was determined by subtracting the initial $H_2O_2$ consumption rate of line b due to the catalase activity from the initial $H_2O_2$ consumption rate of line c. Since the response rate of the $H_2O_2$ sensor (ca. 4 $\mu$M $s^{-1}$) was two orders of magnitude larger than the rate of peroxygenase reaction ($\sim 10^{-2}$ $\mu$M $s^{-1}$) under the present experimental conditions, the response time of the $H_2O_2$ sensor has virtually no effect on the analysis of the peroxygenase activity.

The reaction was analyzed by using kinetic eq 4 derived by steady-state approximation on each intermediate shown in Scheme 3.

$$v^p = \frac{V_{max}}{1 + K_M{}^1/[P] + K_M{}^2/[H_2O_2] + K_M{}^1K_M{}^3/[H_2O_2][P]} \quad (4)$$

$$V_{max} = k_3[E],\ K_M{}^1 = \frac{k_{-2} + k_3}{k_2},\ K_M{}^2 = \frac{k_3}{k_1},\ K_M{}^3 = \frac{k_{-1}}{k_1}$$

where [P] and [E] denote the concentrations of phenol and tyrosinase, respectively. Under the present experimental conditions with the high borate buffer concentration (0.5 M), dissociation of the catechol product from the enzyme active site may be much faster than the other process as in the case

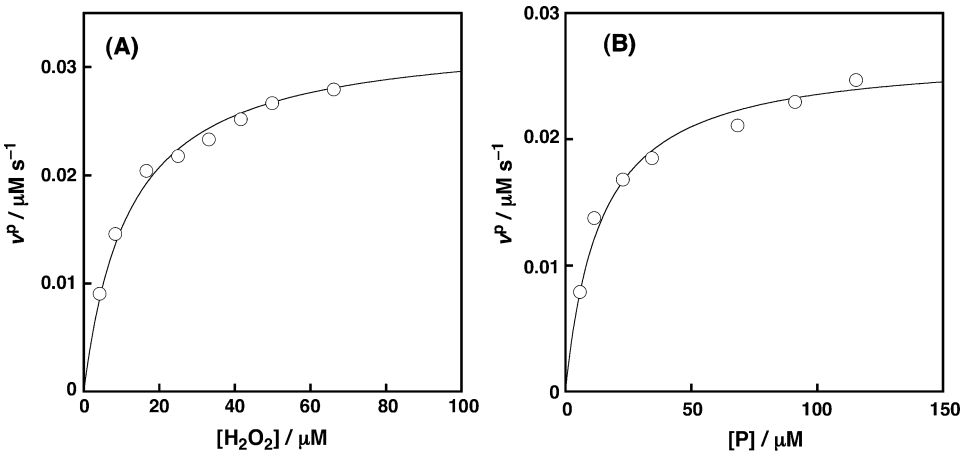


FIGURE 6: (A) Plot of $v^p$ vs [$H_2O_2$] of the oxygenation of *p*-fluorophenol (P) (117 $\mu$M) catalyzed by mushroom tyrosinase (0.135 $\mu$M) in 0.5 M borate buffer (pH 7.0) under $O_2$-saturated conditions and (B) plot of $v^p$ vs [P] of the same reaction at a limited concentration of [$H_2O_2$] = 49.6 $\mu$M.

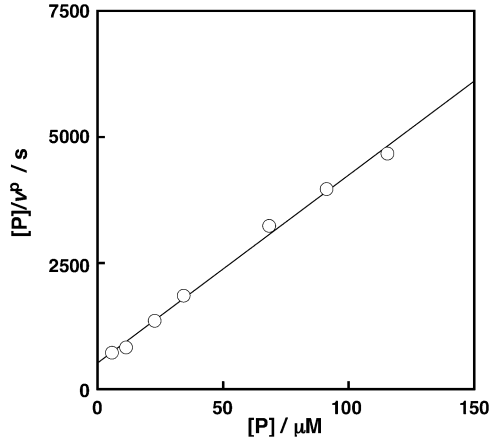


FIGURE 7: Hanes−Woolf plot for the oxidation of *p*-fluorophenol.

of the previous study of phenolase activity (*18*). In Figure 6 is shown the rate dependences on [$H_2O_2$] and [P] in the oxygenation of *p*-fluorophenol (P) as a typical example. As expected from eq 4, the observed rate $v^p$ increases with increasing [$H_2O_2$] at a fixed concentration of [P] = 117 $\mu$M and gradually saturates to reach a constant value at the higher concentration of $H_2O_2$ (Figure 6A). Similarly, $v^p$ increases with increasing [P] at a fixed concentration of [$H_2O_2$] = 49.6 $\mu$M and gradually saturates to reach a constant value at the higher concentration of P (Figure 6B). Then, the reactivity of a series of *p*-substituted phenols has been examined in the presence of the large excess of $H_2O_2$. Under such conditions, $K_M^2/[H_2O_2]$ and $K_M^3K_M^1/[H_2O_2][P]$ terms of eq 4 can be negligible to make the kinetic equation much simpler as eq 5.

$$v^p = \frac{V_{max}}{1 + K_M^1/[P]} \quad (5)$$

From the Hanes−Woolf plot shown in Figure 7 is obtained $V_{max}$ = 0.027 $\mu$M s$^{-1}$ and $K_M^1$ = 1.4 × 10 $\mu$M for *p*-fluorophenol, and the kinetic parameters for other substrates were determined similarly as summarized in Table 1.

Since the reaction was carried out at the fixed high $H_2O_2$ concentration, the $V_{max}$ value might reflect simply the reactivity of the phenol substrate in the oxygen atom transfer process ($V_{max} = k_3$[E]). Thus, $V_{max}$ can be used as an indicator of the peroxygenase activity of tyrosinase. As seen in Table 1, the $V_{max}$ value increases as the electron donor ability of the *p*-substituent increases, and the Hammett plot (log $V_{max}$ vs $\sigma^+$) gave a straight line with a negative slope of −1.7 (Figure 8). This value (Hammett $\rho$ value) is fairly close to that of the phenolase activity of mushroom tyrosinase ($\rho$ = −2.4) (*18*) and nearly identical to the $\rho$ value of our tyrosinase model reaction ($\rho$ = −1.8) (*19*). Moreover, the negative $\rho$ values are indicative of an electrophilic ionic mechanism and are nearly the same to the $\rho$ value of the aromatic ligand hydroxylation reaction with a ($\mu$-$\eta^2$:$\eta^2$-peroxo)dicopper(II) complex via an electrophilic aromatic substitution mechanism ($\rho$ = −2.1) (*20*). Thus, it can be concluded that the peroxygenase activity of tyrosinase involves the electrophilic aromatic substitution mechanism as in the case of phenolase reaction (*18*). In other words,

Table 1: Kinetic Parameters $V_{max}$ and $K_M^1$ for the Peroxygenase Activity of Mushroom Tyrosinase

| *p*-substituent | $K_M^1$ ($\mu$M) | $V_{max}$ ($\mu$M s$^{-1}$) |
|---|---|---|
| Me | 1.8 × 10$^2$ | 0.052 |
| F | 1.4 × 10 | 0.027 |
| Cl | 1.7 × 10 | 0.021 |
| Br | 1.4 × 10 | 0.011 |
| COOMe | [a] − | 0.0022 |

[a] Too small to be determined accurately.

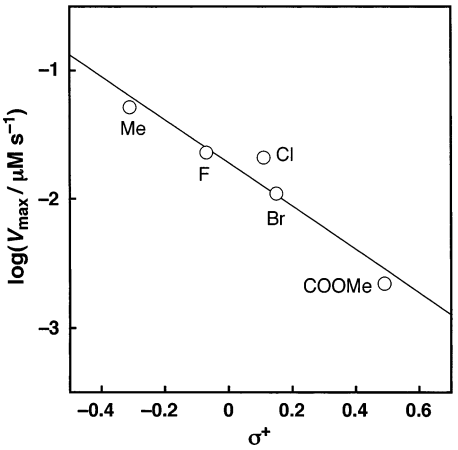


FIGURE 8: Hammett plot for the peroxygenase activity of tyrosinase (data are taken from Table 1).

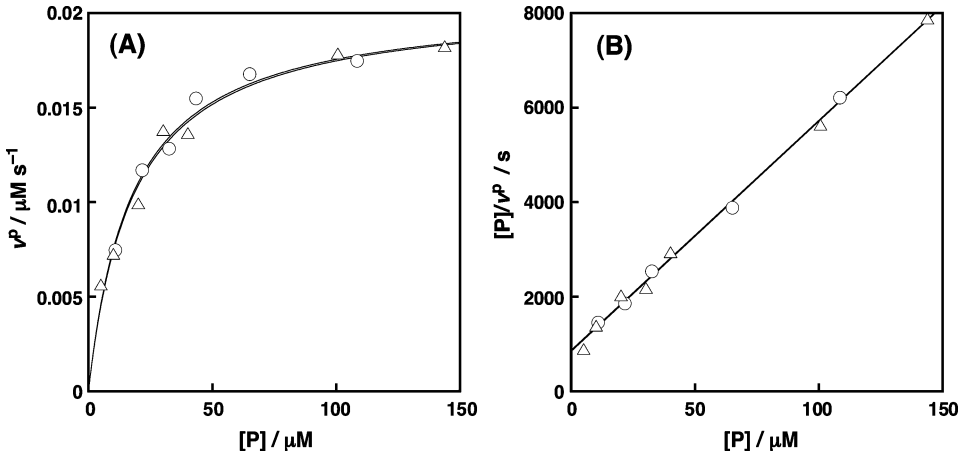


FIGURE 9: (A) Plot of $v^p$ vs [P] for the oxygenation of *p*-Cl-$C_6H_4OH$ (○) and *p*-Cl-$C_6D_4OH$ (△) with $H_2O_2$ (46.9 μM) catalyzed by mushroom tyrosinase (0.135 μM) in 0.5 M borate buffer (pH 7.0) under $O_2$-saturated conditions and (B) their Hanes−Woolf plots.

the ($\mu$-$\eta^2$:$\eta^2$-peroxo)dicopper(II) species is the common active intermediate in both the phenolase reaction and the peroxygenase reaction as indicated in Schemes 1 and 3, respectively. In support of this mechanism, no kinetic deuterium isotope effect was obtained ($V_{max}^H/V_{max}^D = 1.0$) when perdeuterated *p*-chlorophenol *p*-Cl-$C_6D_4OH$ was employed instead of *p*-Cl-$C_6H_4OH$ (Figure 9). In the electrophilic aromatic substitution mechanism (Scheme 1), proton migration from the C−O adduct intermediate would be much faster than the C−O bond formation between the aromatic ring of the substrate and the peroxo species.

In summary, the catalase and peroxygenase activities of mushroom tyrosinase have been explored in detail by using amperometric $O_2$ and $H_2O_2$ sensors. Both activities can be explained by assuming the existence of ($\mu$-$\eta^2$:$\eta^2$-peroxo)-dicopper(II) species as the common reactive intermediate. In the catalase activity, the ($\mu$-$\eta^2$:$\eta^2$-peroxo)dicopper(II) species is formed from met-tyrosinase by the reaction with $H_2O_2$. Then, the dicopper(II)-peroxo complex releases $O_2$ to give deoxy-tyrosinase, with which another molecule of $H_2O_2$ reacts to give met-tyrosinase and $H_2O$, completing the catalytic cycle (Scheme 2). When the phenol substrate is added into the system, the ($\mu$-$\eta^2$:$\eta^2$-peroxo)dicopper(II) species attacks the substrate to induce the C−O bond formation (oxygen atom transfer reaction). The kinetic results (the Hammett plot and the absence of kinetic deuterium isotope effect) have clearly indicated that the reaction involves the electrophilic aromatic substitution mechanism as in the case of phenolase reaction of tyrosinase (*18*). Direct comparison of the catalase activity between mushroom tyrosinase and mollusk hemocyanin has also suggested that the accessibility of substrates to the enzyme active site is critical to control the reactivity of the dinuclear copper site of proteins (*11*). Further studies on the catalase and peroxygenase activities of tyrosinase are currently undertaken to gain more insights into the mechanistic details of the enzymatic reactions.

## ACKNOWLEDGMENT

The authors acknowledge Dr. Yoshimitsu Tachi of Osaka City University for his assistance with the protein purification and electrochemical measurements.

## REFERENCES

1. Solomon, E. I., Sundaram, U. M., and Machonkin, T. E. (1996) Multicopper oxidases and oxygenases, *Chem. Rev. 96*, 2563−2605.
2. Land, E. J., Ramsden, C. A., and Riley, P. A. (2003) Tyrosinase autoactivation and the chemistry of *o*-quinone amines, *Acc. Chem. Res. 36*, 300−308.
3. Fenoll, L. G., Rodríguez-López, J. N., García-Sevilla, F., García-Ruiz, P. A., Varón, R., García-Cánovas, F., and Tudela, J. (2001) Analysis and interpretation of the action mechanism of mushroom tyrosinase on monophenols and diphenols generating highly unstable *o*-quinones, *Biochim. Biophys. Acta 1548*, 1−22.
4. Itoh, S. (2004) Dicopper Enzymes, in *Comprehensive Coordination Chemistry II* (McCleverty, J. A., Meyer, T. J., Eds.) Vol. 8, pp 369−393, Elsevier, Amsterdam.
5. Solomon, E. I., Chen, P., Metz, M., Lee, S., and Palmer, A. E. (2001) Oxygen binding, activation, and reduction to water by copper proteins, *Angew. Chem., Int. Ed. 40*, 4570−4590.
6. van Gelder, C. W., Flurkey, W. H., and Wichers, H. J. (1997) Sequence and structural features of plant and fungal tyrosinases, *Phytochemistry 45*, 1309−1323.
7. Lerch, K. (1987) Molecular and active site structure of tyrosinase, *Life Chem. Rep. 5*, 221−234.
8. Klabunde, T., Eicken, C., Sacchettini, J. C., and Krebs, B. (1998) Crystal structure of a plant catechol oxidase containing a dicopper center, *Nat. Struct. Biol. 5*, 1084−1090.
9. Gerdemann, C., Eicken, C., and Krebs, B. (2002) The crystal structure of catechol oxidase: new insight into the function of type-3 copper proteins, *Acc. Chem. Res. 35*, 183−191.
10. Decker, H., Dillinger, R., and Tuczek, F. (2000) How does tyrosinase work? Recent insights from model chemistry and structural biology, *Angew. Chem., Int. Ed. 39*, 1591−1595.
11. Decker, H., and Tuczek, F. (2000) Tyrosinase/catecoholoxidase activity of hemocyanins: structural basis and molecular mechanism, *Trends Biochem. Sci. 25*, 392−397.
12. van Gastel, M., Bubacco, L., Groenen, E. J. J., Vijgenboom, E., and Canters, G. W. (2000) EPR studies of the dinuclear active site of tyrosinase from *Streptomyces antibioticus*, *FEBS Lett. 474*, 228−232.
13. Bubacco, L., Vijgenboom, E., Gobin, C., Tepper, A. W. J. W., Salgado, J., and Canters, G. W. (2000) Kinetic and paramagnetic NMR investigations of the inhibition of *Streptomyces antibioticus* tyrosinase, *J. Mol. Catal. 8*, 27−35.
14. Bubacco, L., Salgado, J., Tepper, A. W. J. W., Vijgenboom, E., and Canters, G. W. (1999) $^1$H NMR spectroscopy of the binuclear Cu(II) active site of *Streptomyces antibioticus* tyrosinase, *FEBS Lett. 442*, 215−220.
15. Seo, S., Sharma, V. K., and Sharma, N. (2003) Mushroom tyrosinase: recent prospects, *J. Agric. Food Chem. 51*, 2837−2853.
16. Espin, J. C., Varón, R., Fenoll, L. G., Gilabert, M. A., García-Ruiz, P. A., Tudela, J., and García-Cánovas, F. (2000) Kinetic characterization of the substrate specificity and mechanism of mushroom tyrosinase, *Eur. J. Biochem. 267*, 1270−1279.

17. Sánchez-Ferrer, A., Rodríguez-López, J. N., Francisco García-Cánovas, F., and García-Carmona, F. (1995) Tyrosinase: a comprehensive review of its mechanism, *Biochim. Biophys. Acta 1247*, 1−11.
18. Yamazaki, S., and Itoh, S. (2003) Kinetic evaluation of phenolase activity of tyrosinase using simplified catalytic reaction system, *J. Am. Chem. Soc. 125*, 13034−13035.
19. Itoh, S., Kumei, H., Taki, M., Nagatomo, S., Kitagawa, T., and Fukuzumi, S. (2001) Oxygenation of phenols to catechols by a ($\mu$-$\eta^2$:$\eta^2$-peroxo)dicopper(II) complex: mechanistic insight into the phenolase activity of tyrosinase, *J. Am. Chem. Soc. 123*, 6708−6709.
20. Nasir, M. S., Cohen, B. I., and Karlin, K. D. (1992) Mechanism of aromatic hydroxylation in a copper monooxygenase model system. 1,2-Methyl migrations and the NIH shift in copper chemistry, *J. Am. Chem. Soc. 114*, 2482−2494.
21. Pidcock, E., Obias, H. V., Zhang, C. X., Karlin, K. D., and Solomon, E. I. (1998) Investigation of the reactive oxygen intermediate in an arene hydroxylation reaction performed by xylyl-bridged binuclear copper complexes, *J. Am. Chem. Soc. 120*, 7841−7847.
22. Jolley, R. L., Jr., Evans, L. H., and Mason, H. S. (1972) Reversible oxygenation of tyrosinase, *Biochem. Biophys. Res. Commun. 46*, 878−884.
23. Jolley, R. L., Evans, L. H., Makino, N., and Mason, H. S. (1974) Oxytyrosinase, *J. Biol. Chem. 249*, 335−345.
24. Lerch, K. (1976) *Neurospora* tyrosinase: molecular weight, copper content, and spectral properties, *FEBS Lett. 69*, 157−160.
25. Eickman, N. C., Solomon, E. I., Larrabee, J. A., Spiro, T. G., and Lerch, K. (1978) Ultraviolet resonance Raman study of oxytyrosinase. Comparison with oxyhemocyanin, *J. Am. Chem. Soc. 100*, 6529−6531.
26. Ghiretti, F. (1956) The decomposition of hydrogen peroxide by hemocyanin and by its dissociation products, *Arch. Biochem. Biophys. 63*, 165−176.
27. Felsenfeld, G., and Printz, M. P. (1959) Specific reaction of hydrogen peroxide with the active site of hemocyanin. The formation of methemocyanin, *J. Am. Chem. Soc. 81*, 6259−6264.
28. Himmelwright, R. S., Eickman, N. C., LuBien, C. D., and Solomon, E. I. (1980) Chemical and spectroscopic comparison of the binuclear copper active site of mollusc and arthropod hemocyanins, *J. Am. Chem. Soc. 102*, 5378−5388.
29. Zlateva, T., Santagostini, L., Bubacco, L., Casella, L., Salvato, B., and Beltramini, M. (1998) Isolation of the met-derivative intermediate in the catalase-like activity of deoxygenated *Octopus vulgaris* hemocyanin, *J. Inorg. Biochem. 72*, 211−215.
30. Gerdemann, C., Eicken, C., Magrini, A., Meyer, H. E., Rompel, A., Spener, F., and Krebs, B. (2001) Isozymes of *Ipomoea batatas* catechol oxidase differ in catalase-like activity, *Biochim. Biophysis. Acta 1548*, 94−105.
31. Kinoshita, H., Torimura, M., Kano, K., and Ikeda, T. (1997) Peroxidase-based amperometric sensor of hydrogen peroxide generated in oxidase reaction: application of creatinine and creatine assay, *Electroanalysis 9*, 1234−1238.
32. Mochizuki, M., Yamazaki, S., Kano, K., and Ikeda, T. (2002) Kinetic analysis and mechanistic aspects of autoxidation of catechins, *Biochim. Biophys. Acta 1569*, 35−44.
33. James, T. D., Sandanayake, K. R. A. S., and Shinkai, S. (1995) Recognition of sugars and related compounds by reading-out-type interfaces, *Supramol. Chem. 6*, 141−157.
34. Jallal, M. G., and Roger, A. S. (1995) Highly regioselective ortho-chlorination of phenol with sulfuryl chloride in the presence of amines, *Tetrahedron Lett. 36*, 3893−3896.
35. Osako, T., and Itoh, S (2004) Reaction of copper(I) complex and $H_2O_2$, unpublished results.
36. Cuff, M. E., Miller, K. I., van Holde, K. E., and Hendrickson, W. A. (1998) Crystal structure of a functional unit from *Octopus* hemocyanin, *J. Mol. Biol. 278*, 855−870.
37. Hazes, B., Magnus, K. A., Bonaventura, C., Bonaventura, J., Dauter, Z., Kalk, K. H., and Hol, W. G. J. (1993) Crystal structure of deoxygenated *Limulus polyphemus* subunit II hemocyanin at 2.18 Å resolution: Clues for a mechanism for allosteric regulation, *Protein Sci. 2*, 597−619.

BI048908F